

## Thermodynamic analyses of film cooling from compound spherical trenched holes at the end of combustor simulator

Ehsan Kianpour<sup>1\*</sup>, Nor Azwadi Che sidik<sup>2</sup>

1 -Department of Mechanical Engineering, Najafabad Branch, Islamic Azad University, Najafabad, Iran, ekianpour@pmc.iaun.ac.ir

2 -Department of Thermo-fluid, Faculty of Mechanical Engineering, University Technology of Malaysia, Johor, Malaysia, azwadi@utm.my

\*Corresponding author

### Abstract

The major effects of cylindrical and spherical trenched cooling holes with distance between the hole surface and the combustion chamber panel and the filler diameter on the spherical hole contact surface and the panel surface  $H=0.2, R=D/2=0.2$ ,  $H=0.3, R=D/2=0.2$  and  $H=0.4, R=D/2=0.2$  cm at  $BR=3.18$  on the film cooling effectiveness near the combustor end wall surface is an important subject to study in detail. This research included a three-dimensional representation of a Pratt and Whitney gas turbine engine was simulated and analyzed with a commercial finite volume package FLUENT 6.2.26. This analyze was done with RANS turbulence model on internal cooling passages. This combustor simulator was combined with the interaction of two rows of dilution jets, which were staggered in the streamwise direction and aligned in the spanwise direction. In comparison with the baseline case, the application of trenched holes increased the effectiveness of film cooling up to 47% near the wall surface and an average of 35% in depth of combustor simulator.

**Keywords:** Gas Turbine Engine, Film-Cooling, Trench Hole, Dilution Hole

### Introduction

Advanced gas turbine industries are trying hard for higher engine efficiencies. Brayton cycle is a key to achieve this purpose. In this cycle, to have higher gas turbine engine efficiency, the combustor's outlet temperature must increase [1]. But such hot flows cause non-uniformities at the end of the combustor and the inlet of the turbine and damage the critical parts. Film cooling is the most well-known method of preservation. In this technique, a low temperature thin layer attaches on a surface and protects it against hot streams. To get better film cooling performance, it is needed to increase blowing ratio. Blowing ratio increment has an intense effect on the heat transfer, particularly in the hole region. According to the importance of this study, a broad literature survey was done to get the Fundamental data. Harrington et al. [2] presented a simulated flat plate. The research was a computational and experimental one aimed at investigating a full coverage of adiabatic film cooling effectiveness. The focus of the findings was on the effects of ten rows of normal short cooling holes with a length of  $l/D = 1.0$  at large density coolant jets and high mainstream

turbulence intensity. The test results indicated that considering the blowing ratio, the maximum adiabatic film cooling effectiveness was attained near the area, which covered four to eight rows of cooling holes. Furthermore, the interaction of injected flows sprayed from the cooling rows limits the maximum effectiveness. On the other hand, film cooling effectiveness on the curved surface was investigated numerically by Koc et al. [3]. They highlighted that the curvature of the surface and the blowing ratio affect the film cooling effectiveness. In another study, Azzi and Jurban [4] forecasted the film cooling thermal fields for a simulated cylindrical cooling row with the following ratios: extended range of length to diameter =  $1.75/8$ , and fixed pitch to diameter =  $3.0$ . The inclination angle was  $35$  degrees and the film hole was  $12.7$  mm in diameter. Another finding by Bernsdorf et al., [5] showed that in short cooling injection holes, effectiveness of film cooling is related to the injection hole length and angle. Tarchi et al. [6] investigated the effects of large dilution holes. These holes were placed within the injecting slot and eruption array. The flat plate cross section duct contained 270 cooling holes located in 29 staggered rows. The holes were  $1.65$  mm in diameter and had a length to diameter ratio of  $5.5$  and a stream-wise angle of  $30$  degrees. The dilution hole was  $18.75$  mm in diameter. It was located at the 14<sup>th</sup> row of cooling holes. They showed that with using backward step, at downstream the dilution hole the adiabatic film cooling effectiveness reached to  $\eta_{aw}=0.65$ . Vakil and Thole [7] presented experimental results of the study of temperature distribution inside a combustor simulator. In this study, a real large scale of combustor was modelled. This model contained four different cooling panels with many cooling holes. Two rows of dilution jets could be seen in the second and third cooling panels. The first row had three dilution jets and the second one had two jets. While the first and second panels were flat, two other panels angled with an angle of  $15.8$  degrees. In this study, a real large scale of combustor was simulated and high momentum dilution jets and the coolant flow were injected into the main flow. The results indicated that high temperature gradient was developed upstream of the dilution holes. Kianpour et al. [8,9] re-simulated the Vakil and Thole's combustor. They offered various geometries of cooling holes. The temperatures near the wall and among the jets were

higher for the baseline cooling whereas the central part of the jets was cooler in trench cases. In one study, Schuchkin et al. [10] investigated film cooling effectiveness in ultrasonic flow. The results showed that with Mach number increasing, shell friction coefficient, diffusion ratio, and turbulence intensity at the boundary film cooling decreased. Porosity reduces shell friction and mixing and thus improving the cooling effectiveness of the layer. In 2018, Li et al. [11] numerically studied the film cooling effectiveness of a layer with shaped holes during the end cross-flows of the end wall. They found that despite the creation of negative vortices and jet vortices in the internal crossover flow resulting from the simulation of the flow in the turbine blade environment, the reuse of these end wall currents affects the film cooling effectiveness. Fraas et al. [12] experimentally studied the film cooling performance improvement by using an optimized cooling hole inlet geometry. The results showed that the cooling hole inlet geometry tremendously affects cooling performance. Diffuser aerodynamics are altered for all investigated geometries with a modified inlet. This leads to a more symmetrical pattern of the film cooling jet for two of the investigated geometries. Chen et al. [13] studied film cooling effectiveness distribution for a gas turbine blade under the effects of unsteady wakes and oncoming free-stream turbulence intensities using pressure sensitive paint (PSP) technique. Results showed that the effect of the mass flux ratio on the film cooling effectiveness decreases under the high turbulence intensity and unsteady wake conditions. Kim et al. [14] experimentally studied the effects of a protrusion installed at the slot exit on the film cooling effectiveness of inclined slots. Injection angles of  $30^\circ$  and  $45^\circ$  were considered for the slot, and a protrusion that induces the effects of free jet emerges close to a surface was installed at the slot exit. The film cooling effectiveness of the  $45^\circ$  inclined slot was improved by about 6.6% by installing a protrusion immediately after the slot exit.

### Research Methodology

In the present study, the combustor simulator applied was a 3-D representation of a Pratt and Whitney gas turbine engine. In a real combustor, film cooling jets are used to form a low temperature layer of air that covers the combustor's inner and outer coating. Without effective cooling, this cover is going to melt and cause disaster effects. The combustor was a three-dimensional container. The width, height and length of this container was 111.8cm, 99.1cm and 156.9cm respectively. The container converged from  $X/L=0.51$  and contraction angle was 15.8 degrees. Inlet and outlet cross-sectional area of the combustor simulator was  $1.11\text{m}^2$  and  $0.62\text{m}^2$ . The test section contained two symmetric surfaces on the top and bottom of the combustor but the fluid only flowed through bottom passage. The lengths of the panels were 39cm, 41cm, 37 and 43 centimeters

respectively. In addition, the first two panels were flat and have constant sectional area. However, the last two panels were inclined at the contraction angle and yield the exit sectional area of the combustor simulator. The panels were 1.27cm thick, and due to the low thermal conductivity ( $k=0.037\text{ W/mk}$ ), adiabatic surface temperature measurements were possible. Dilution flow injection is beneficial to decline the temperature of the hot exit gases of the combustor simulator and prevent the detrimental effects of the critical components. Two different dilution rows were considered within the second and third panel of cooling panels. The dilution flow injected into the mainstream flow vertically, while, the dilution hole in the third panel was angled at 15.8degrees from the vertical axis. The first row of dilution jets included three holes and it was placed at 0.67m downstream of the combustor simulator inlet. These holes were 8.5cm in diameter. The second row contained two dilution holes and was located at 0.23m downstream of the first row of dilution holes center. These holes diameter was 1.4 times more than the first one at 12.1cm. The centerline of the second row was staggered with respect to those of the first row. In the present research, the combustor simulator contained four arrangements of cooling holes. For the verification of findings, the first arrangement (baseline or case 1) was designed similar to the Vakili and Thole [7] combustor simulator. As seen in Figure 1, The length of these cooling holes was 2.5cm and they drilled at an angle of  $30^\circ$  from the horizontal surface.

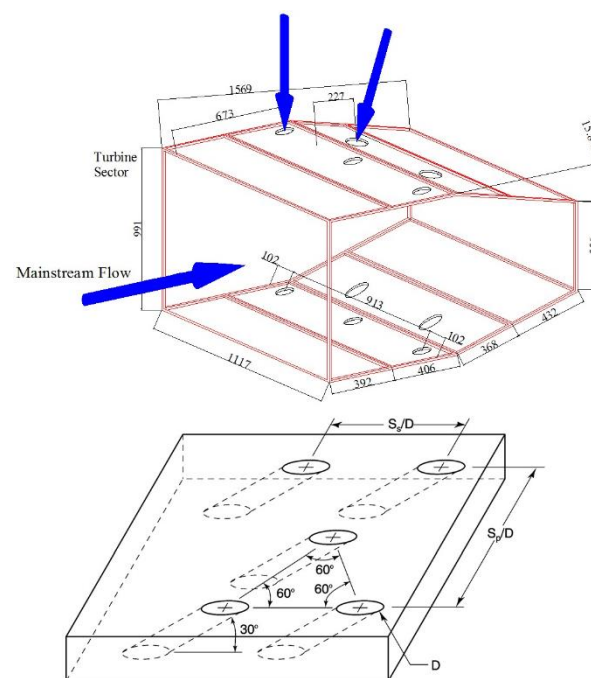


Figure 1. (a) Schematic view of the combustor simulator (b) film cooling holes arrangement

The film-cooling holes were 0.76cm in diameter. Except the baseline case which introduced, to investigate the effects of cooling holes trenching,

trenched spherical holes were considered. These holes have an elliptical cross section at the entrance of the cooling holes and starts to expand at a certain angle in a part of the hole path line and at the end of the cooling hole reaches to a new cross section shape (Figure 2). The distance between the hole surface and the combustion chamber panel and the filler diameter on the spherical hole contact surface and the panel surface  $H=0.2, R=D/2=0.2$ ,  $H=0.3$ ,  $R=D/2=0.2$  and  $H=0.4$ ,  $R=D/2=0.2$  cm. Other geometric parameters of cooling holes are shown in Table 1.

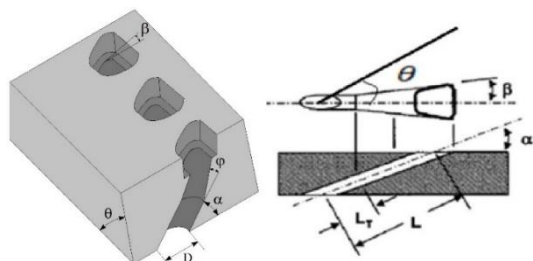


Figure 2. (a) Schematic view of the combustor simulator (b) film cooling holes arrangement

Table 1. Geometric parameters of cooling holes

parameter	quantity
$\beta$	$0.6 \alpha$
$\theta$	$\alpha$
L (cm)	2.5
$L_r/L$	0.4
H	$0.8D$

The Cartesian coordinate system (x, y and z) was selected. All coordinates were non-dimensionalized by the combustor simulator height ( $H_{in}$ ), length (L) and width (W) respectively. The temperature of coolant and dilution jets was equal to 295.5 K. The temperature of mainstream was 332K. Figure 3 shows the observation planes which are used to measure the film-cooling effectiveness distribution for baseline case and three different configurations of row trenched cooling holes. The observation planes of P0, P1, P2, and P3 and S0 were placed in pitch wise and streamwise direction respectively. Plane P0 was located at  $x=35.1$  cm. The distribution of film cooling momentum was computed along this panel. This plane lengthened within half of the combustor in the spanwise direction. The observation plane height extended from  $z=0$ cm to  $z=10$ cm. Plane P1 was located at the trailing edge of the first row of dilution jet. The importance of this plane was to identify the stream-wise behavior of the dilution jets first row. About  $8 \times 10^6$  tetrahedral meshes were selected (Figure 4). This quantity of nodes allowed appropriate convergence for corrected meshing; the thermal and flow characters would have the similar variation as the higher refinement mesh.

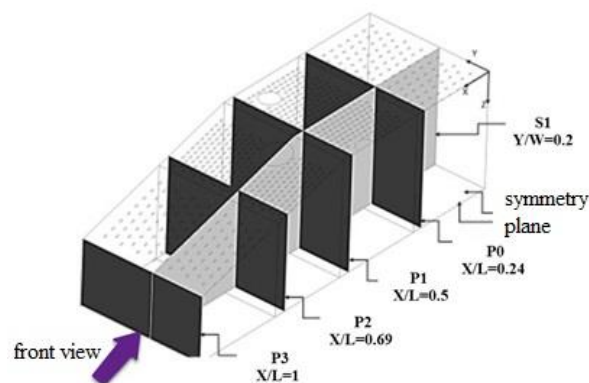


Figure 3. Schematic view of the observation planes

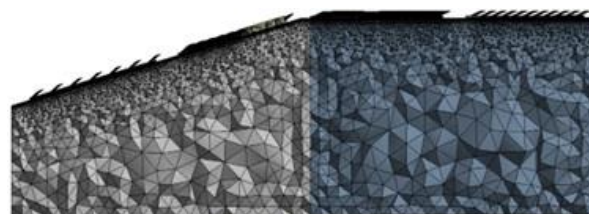


Figure 4. Meshes of combustor simulator

According to the considered blowing ratio at the inlet of control volume, the boundary condition of inlet mass flow was considered at the inlet. to limit the interaction region between fluid and combustor wall, slip-less boundary condition and wall boundary condition were considered. In addition, two different boundary conditions of uniform flow and pressure outlet was selected at the inlet and outlet of combustor respectively. Totally, according to the symmetries of the Pratt and Whitney gas turbine engine combustor, symmetry boundary condition was used. Gambit package was selected to mesh the combustor simulator and the model was analyzed by Fluent 6.2.26 software. It then makes a comparison in regard to the thermal field between numerical studies done by the finite difference method and the computational analyses previously performed by Vakil and Thole [13] and Stitzel and Thole [20]. The numerical method considered a transient, incompressible turbulent flow by means of the k-ε turbulent model of the Navier–Stokes equations expressed as follows:

Continuity equation

$$\frac{\partial}{\partial t}(\rho u_i) + \frac{\partial}{\partial x_j}(\rho u_i u_j) = -\frac{\partial p}{\partial x_i} + \frac{\partial \tau_{ij}}{\partial x_i} + \rho g_i + \vec{F}_1 \quad (1)$$

Momentum equation

$$\frac{\partial \rho}{\partial t} + \frac{\partial \rho}{\partial x} \frac{dx}{dt} + \frac{\partial \rho}{\partial y} \frac{dy}{dt} + \frac{\partial \rho}{\partial z} \frac{dz}{dt} = -\rho(\nabla \cdot V) \quad (2)$$

Energy equation

$$\frac{\partial}{\partial t}(\rho E) + \frac{\partial \rho}{\partial x_j} = (u_i(\rho E + P)) = \frac{\partial}{\partial x_i} \left( K_{eff} \frac{\partial T}{\partial x_i} - \sum_j h_j J_j + u_i(\tau_{ij})_{eff} \right) + S_h \quad (3)$$

and k-ε equation

$$\frac{\partial}{\partial t}(\rho k) + \frac{\partial}{\partial x_i}(\rho k u_i) = \frac{\partial}{\partial x_i} \left( \mu + \frac{\mu_t}{\sigma_k} \frac{\partial k}{\partial x_i} \right) + P_k - \rho \epsilon \quad (4)$$

$$\frac{\partial}{\partial t}(\rho \epsilon) + \frac{\partial}{\partial x_i}(\rho \epsilon u_i) = \frac{\partial}{\partial x_j} \left( \left( \mu + \frac{\mu_t}{\sigma_\epsilon} \right) \frac{\partial \epsilon}{\partial x_j} \right) + C_{1\epsilon} \frac{\epsilon}{k} P_k - C_{2\epsilon}^* \rho \frac{\epsilon^2}{k} \quad (5)$$

The convective and diffusion terms were approximated by the first-order upwind and central differencing scheme. To investigate the convergence limit, the control volume mass residue has been estimated and the maximum value has been used. For this research, the criterion of convergence has chosen  $10^{-4}$ . The following equation is to determine the effectiveness of film cooling.

$$\eta = T - T_\infty / T_c - T_\infty \quad (6)$$

Here  $T$ ,  $T_\infty$  and  $T_c$  is the local temperature, the temperature mainstream and coolant respectively.

**Findings and Discussion**

The findings of the current research were compared with the experimental collected results which was done by Vakil and Thole [7]. The effectiveness of film-cooling was compared in plane P1 at  $y/w=0.25$  (Figure 5). The deviations between the results of current research and benchmarks were computed by the following equation.

$$\%Diff = \left( \frac{\sum_{j=1}^n \frac{x_i - x_{i,benchmark}}{x_{i,benchmark}}}{n} \right) \times 100 \quad (7)$$

The deviation was equal to 5% compared to Vakil and Thole measurements [7] for plane P1.

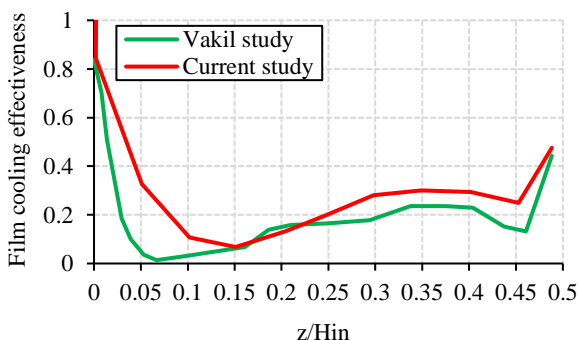


Figure 5. The film cooling effectiveness comparison of plane P1 along  $y/W=0.25$

Figures 6 and 7 show the averaged film cooling effectiveness at different trench heights from 0.2 to

0.4 and constant radius on observation planes P1 and P2. As can be seen, in the middle of the combustor simulator and at a distance of  $0.01\text{cm} < z < 0.04\text{cm}$ , with  $H=0.3$  and  $R=0.2$  cm, a spherical hole has the highest film cooling effectiveness. At the end of the combustor simulator, the film cooling effectiveness is similar for all three types of trench spherical holes. This indicates an increase in the penetration of the dilution jets into the spherical hole with  $H=0.3$  and  $R=0.2$  cm, which improves the film cooling effectiveness in the combustor simulator. According to the results obtained from numerical analyzes, the application of spherical trenched holes with different heights will increase the film cooling effectiveness and reduce the temperature of the combustor simulator. On the other hand, along the combustor, the spherical hole with  $H=0.3$  and  $R=0.2$  cm has the highest film cooling effectiveness.

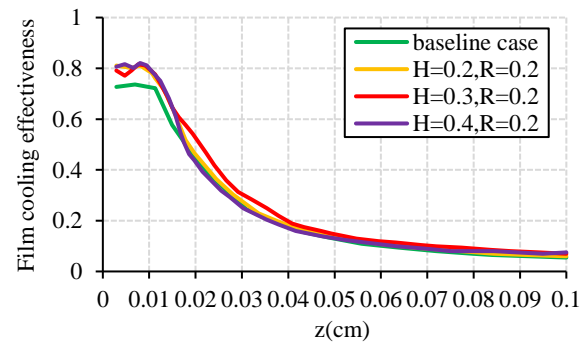


Figure 6. Averaged film cooling effectiveness distribution for plane P1

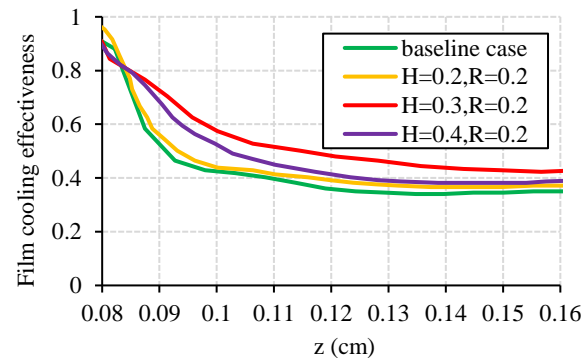


Figure 7. Averaged film cooling effectiveness distribution of plane P2

The effectiveness of film cooling in observation plane P2 at blowing ratio of 3.18 is shown in Figure 8. The most important difference between these schemes is the coolant injection into the main flow. Exactly downstream the second row of dilution jets, more effective coolant layer ( $10\text{cm} < y < 50\text{cm}$ ) was formed by the trenched holes with  $H=0.3$  and  $R=0.2$  cm on the critical surfaces downstream the combustor simulator. The significant protective layer ( $0.9 < \eta < 1.0$ ) was seen for the row trenched holes with  $H=0.3$  and  $R=0.2$  cm. Also, the results show that at height of  $H=0.4$  and  $H=0.2\text{cm}$ , the cooling



absorption of the layer adjacent to the wall is weaker. The reason for this is to reduce the penetration of the cooling current due to the reduction of the flow turbulence. This reduces heat transfer and weakens the film cooling on the combustion chamber panels. For the trenched holes with  $H=0.3$  and  $R=0.2$  cm, the maximum height of the layer was 20 cm, equal to 20% of the combustor inlet height. This gave the highest cooling layer among all the cases.

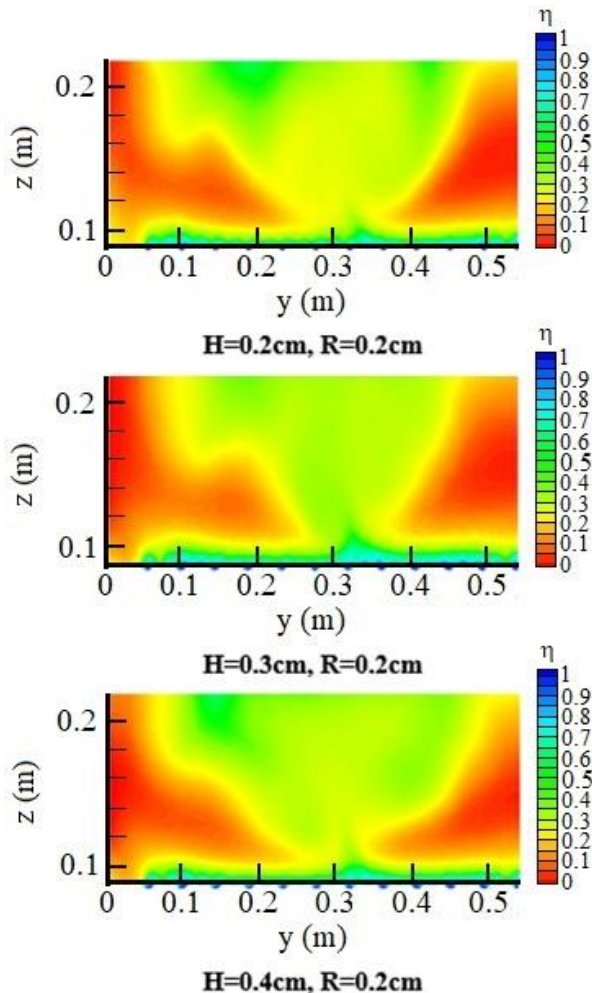


Figure 8. Film cooling effectiveness in plane P2

In Figure 9, the film cooling effectiveness distribution on the observation plane of S1 at different heights from  $H=0.2$ cm to  $H=0.4$ cm and constant radius  $R=0.2$  cm is shown. As can be seen, the spherical hole with  $H=0.2$ cm and  $R=0.2$ cm has the lowest film cooling effectiveness throughout the combustor simulator. As can be seen, the temperature contours immediately behind the jet show a thinner layer of film cooling when the flow is entrained into the jet. Much of the film-coolant was entrained and carried away by the dilution jet right at the trailing edge, thus leaving behind a thinner film of coolant. This entrainment, or recirculating region behind the dilution jet, could also be seen within observation plane of S1. In the first half of the combustion chamber, at  $0m < z < 0.3m$ , the cooling

efficiency of the cavity with  $H=0.4$ cm is higher and has a higher cooling effectiveness. But in the second half of the combustion chamber, at  $0.3m < z < 0.5m$ , this procedure is reversed and the cooling effectiveness of the hole with  $H=0.3$ cm is higher and has a higher cooling effectiveness.

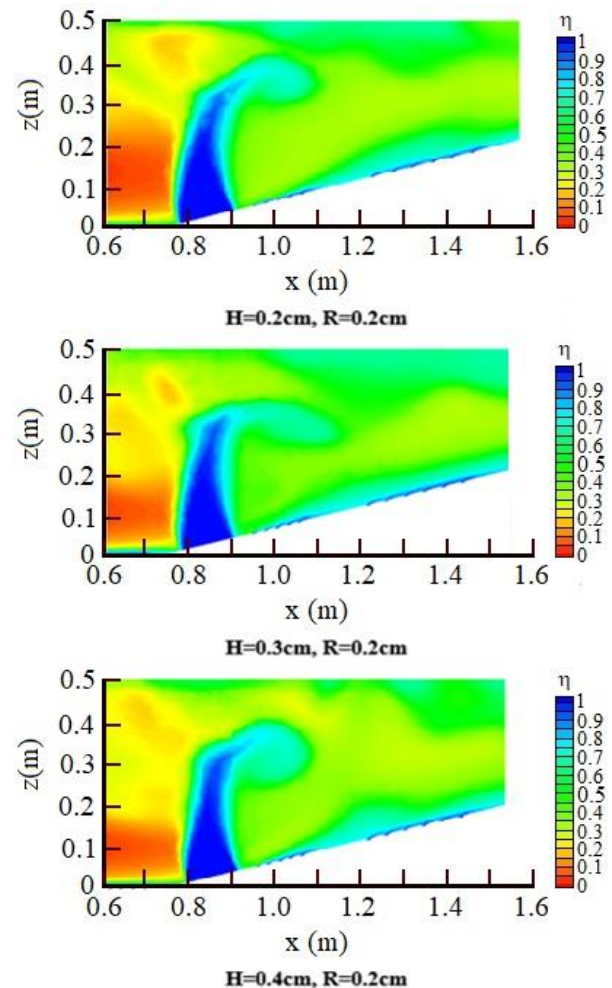


Figure 9. Film cooling effectiveness of plane S1

**Conclusions**

In this research a computational study was conducted in order to have a better understanding of the film cooling effectiveness and the effects of cylindrical and spherical trenched cooling holes with surface  $H=0.2, R=D/2=0.2$ ,  $H=0.3, R=D/2=0.2$  and  $H=0.4, R=D/2=0.2$  from the combustor exit of a gas turbine engine at  $BR=3.18$ . An optimize design cooling holes will help to maximize the effectiveness of cooling along the combustor end wall surface and prevent premature wear in this area. A three-dimensional representation of a gas turbine engine was simulated in order to analyse the effects of cylindrical spherical trenched cooling holes on film cooling performance. The combustor simulator combined the effects of two rows of stream-wise staggered and span-wise aligned dilution jets. The commercial FLUENT software and RNG k-ε turbulence model were employed to run the computations on the thermal fields within a

combustor simulator. Compared to baseline method, in the trenched case, the coolant stayed closer to the end wall surface and did not allow main entrainment. Comparisons between the data computationally predicted and those collected by Vakil and Thole [7] indicate the existence of similarities and differences. The results show that it is more desirable to use this hole geometry so that the film cooling effectiveness increase in about 48 percent on observation planes of P1 and P2.

## References

- [1] Elmahi, A., Baki, T., Tebbal M., 2021, "New analysis of experimental data of the hydrodynamic liquid film around jet zone on horizontal plate", *Archive of Mechanical Engineering*, **68**, 435-448
- [2] Harrington, M. K., McWaters, M. A., Bogard, D. G., Lemmon, C. A., Thole, K. A., 2001, "Full-Coverage Film Cooling With Short Normal Injection Holes", *Journal of Turbomachinery*, **123**, 798-805
- [3] Koc, I., Parmaksızoglu, C., Cakan, M., 2009, "Investigation of film cooling effectiveness and heat transfer coefficient for rectangular holes with two rows", *Energy Conversion and Management*, **81**, 106-117
- [4] Azzi, A., Jubran, B. A., 2003, "Numerical Modeling of Film Cooling from Short Length Stream-Wise Injection Holes", *International Journal of Heat and Mass Transfer*, **39**, 345-353
- [5] Bernsdorf, S., Rose, M., Abhari, R. S., 2006, "Modeling of Film Cooling—Part I: Experimental Study of Flow Structure", *Journal of Turbomachinery*, **128**, 141-149
- [6] Tarchi, L., Facchini, B., Maiuolo, F., Coutandin, D., 2012, "Experimental Investigation on the Effects of a Large Recirculating Area on the Performance of an Effusion Cooled Combustor Liner", *Journal of Engineering for Gas Turbines and Power*, **134**, 041505-1-041505-9
- [7] Vakil, S. S., Thole, K. A., 2005, "Flow and Thermal Field Measurements in a Combustor Simulator Relevant to a Gas Turbine Aero engine", *Journal of Engineering for Gas Turbines and Power*, **127**, 257-267
- [8] Azwadi, N., Kianpour, E., 2014, "The Effect of Blowing Ratio on Film Cooling Effectiveness Using Cylindrical and Row Trenched Cooling Holes with Alignment Angle of 90 Degrees", *Mathematical Problems in Engineering*, Article ID 470576
- [9] Kianpour, E., Sidik, N. A. C., Bozorg, M. A. S. M., 2012, "Thermodynamic Analysis of Flow Field at the End of Combustor Simulator", *Applied Mechanics and Materials*, **225**, 261-266
- [10] Schuchkin, V., Osipov, M., Shyy, W., Thakur, S., 2002, "Mixing and film cooling in supersonic duct flows", *International journal of heat and mass transfer*, **45**, 4451-4461
- [11] Li, Y., Zhang, Y., Su, X., Yuan, X., 2018, "Experimental and numerical investigations of shaped hole film cooling with the influence of endwall cross flow", *International Journal of Heat and Mass Transfer*, **120**, 42-55
- [12] Fraas, M., Glasenapp, T., Schulz, A., Bauer, H. J., 2019, "Optimized inlet geometry of a laidback fan-shaped film cooling hole—experimental study of film cooling performance", *International Journal of Heat and Mass Transfer*, **128**, 980-990
- [13] Chen, D. W., Zhu, H. R., Liu, C. L., Li, H. T., Zhou, D. E., 2019, "Combined effects of unsteady wake and free-stream turbulence on turbine blade film cooling with laid-back fan-shaped holes using PSP technique", *International Journal of Heat and Mass Transfer*, **133**, 382-392
- [14] Kim, S. M., Lee, K. D., Kim, K. Y., 2012, "A comparative analysis of various shaped film-cooling holes", *Heat and Mass Transfer*, **48**, 1929-1939